ANNALI DI GEOFISICA, VOL. XL, N. 2, March 1997

Electrotelluric noise minimization for seismoelectric effect detection

Boris Shirman([1])([2]) **and Avi Shapira**([1])
([1]) *Seismology Division, Institute for Petroleum Research and Geophysics, Holon, Israel*
([2]) *Research Department, Survey of Israel, Tel-Aviv, Israel*

Abstract
Three electrotelluric stations were installed in Israel in order to examine electric field changes associated with earthquake occurrence at the Bar-Giora observatory, at the Ein Gedi field school and on Mt. Tur'an. During the observation period 1994-1995, no earthquake was shown to cause any changes in the electric field at the measurement sites. This study focused on signal processing of electric field continuous measurements. The main purpose was to identify, and consequently filter out, signals caused by local and extra-terrestrial sources. New procedures for data processing were developed mainly using data from the Bar-Giora station, which has been instrumental in the experiments.

Key words *magnetotelluric field – electrodes – noise filtration – earthquake occurrence*

1. Introduction

Electrotelluric field variations are monitored by networks of field stations in Greece and Japan employed for earthquake prediction (Varotsos and Alexopoulos, 1984a,b; Kinoshita *et al.*, 1989). Interest in the electrotelluric effects preceding an earthquake has grown recently (Maron *et al.*, 1993; Di Bello *et al.*, 1994). Electrotelluric field monitoring to detect seismoelectric effects began in 1993-1994 at three stations located near the Dead sea transform fault system. Identical equipment and data acquisition software have been installed at all three stations. Each pair of lead electrodes is connected to a PC based data acquisition system which can record potential differences in a range of about ± 330 mV with a resolution of about 0.16 mV. Data are sampled once per second and averaged over one minute. The average values are continuously stored on hard disk (Shirman and Shapira, 1994).

The main objective of data processing is to recognize and remove noise in the electric field in order to identify variations associated with seismotectonic processes. Our experience of magnetotelluric field monitoring as well as the results of other researchers (Maron *et al.*, 1993; Di Bello *et al.*, 1994) have enabled us to identify three main sources of electrotelluric noise:

1) local electrochemical currents around the electrodes (associated with changes in meteorological conditions);

2) anthropogenic (or industrial) noise (electricity supply lines, factories, etc.);

3) external sources: variations in the Earth's outer magnetic field (solar day variations, magnetic storms, etc.).

Mailing address: Dr. Boris Shirman, Seismology Division, Institute for Petroleum Research and Geophysics, P.O. Box 2286, Holon 58122, Israel; e-mail: seis@iprg.energy.gov.il

Measurements of the electric field at the three monitoring stations Bar-Giora (magnetic observatory), Mt. Tur'an and Ein Gedi were routinely compared with the seismic activity in the region. Earthquake bulletin information and the seismicity map (see fig. 1, where triangles denote station locations) show that no earthquake of a magnitude significant to our study occurred during the period under consideration. Hence, our attention focused on a solution to the noise minimization problem in the absence of a desired signal.

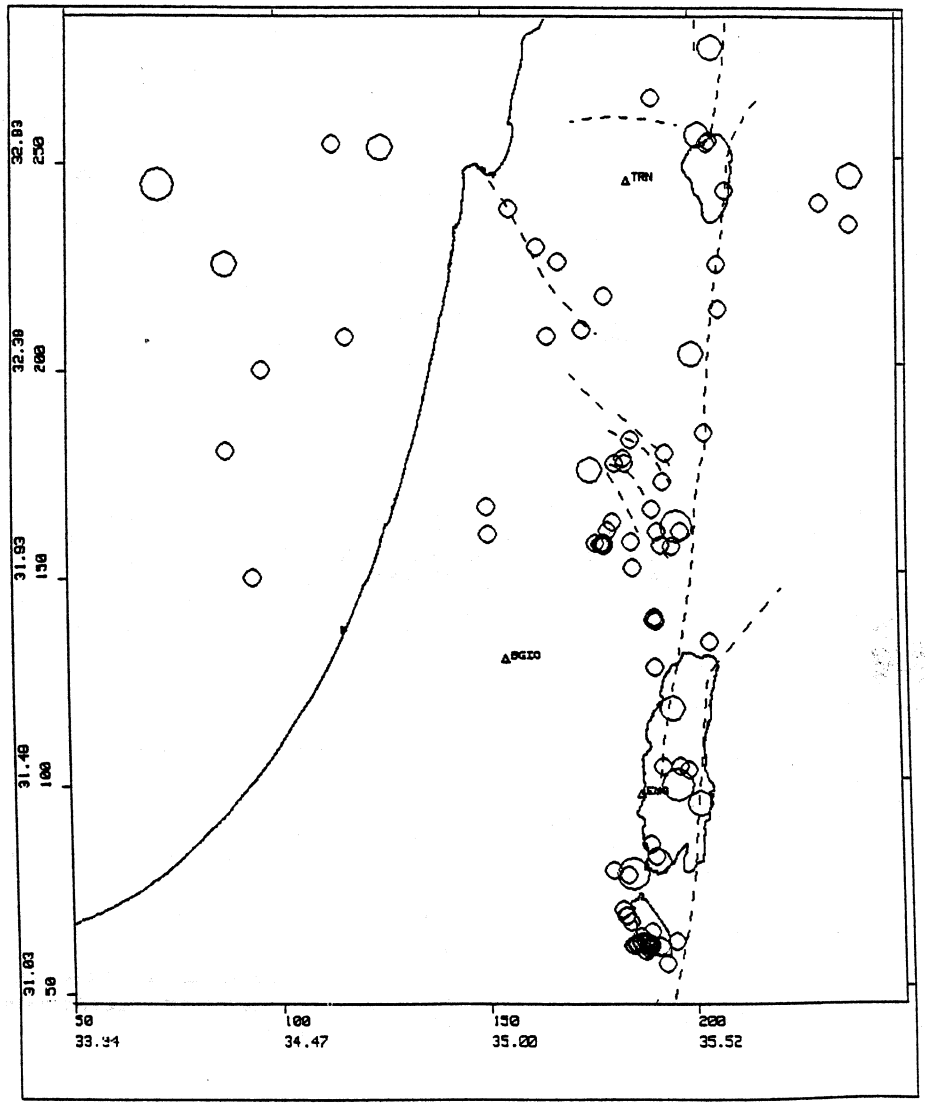

Fig. 1. Map of epicenter locations of earthquakes occurring in Israel from January 1993 to August 1995 ($4 > M > 2$).

2. A new approach to electrochemical local variation minimization

2.1. *Physical principle*

Electrochemical Local Variations (ELV) are caused by special electrochemical polarization processes between electrodes and soil. The electrode charge depends on meteorological conditions (*i.e.*, rainfall, soil temperature and humidity, solar radiation, etc.). Our approach to ELV detection is based on the electrotelluric field observations obtained using two disk-shaped, lead electrodes of different sizes deployed at each of the holes in N-S and E-W directions and then comparing the electric potentials of adjacent electrodes. The electric potential of an electrically charged conductor (thin disk) is defined as:

$$\Phi = q/C$$

where $C = 2a/\pi$ is the electric capacity, q is the full charge, a is the radius of the disk. Hence:

$$\Phi = \pi q/2a \qquad (2.1)$$

An equipotential electric field on an electrode surface must be provided by surface charge density (Jackson, 1962):

$$\sigma(r) = q/(2\pi a(\sqrt{(a^2 - r^2)})). \qquad (2.2)$$

We assume that the surfaces of the two different electrodes deployed in the same hole are in identical electrochemical conditions, therefore, according to electrode symmetry, the charge density in the centers of the disks is equivalent to:

$$\sigma(0) = \frac{q}{2\pi a^2} = \frac{\overline{\sigma}}{2} = \sigma_0 = \text{const.} \qquad (2.3)$$

Introducing eq. (2.3) to eq. (2.1), we find that the electric potential is proportional to the electrode radius:

$$\Phi = \pi^2 \sigma_0 a. \qquad (2.4)$$

Consequently, the potential differences between two adjacent electrodes with different radii represent the electrochemical change of electrodes in the given hole (electric potentials of two nearby electrodes of other sources are equivalent).

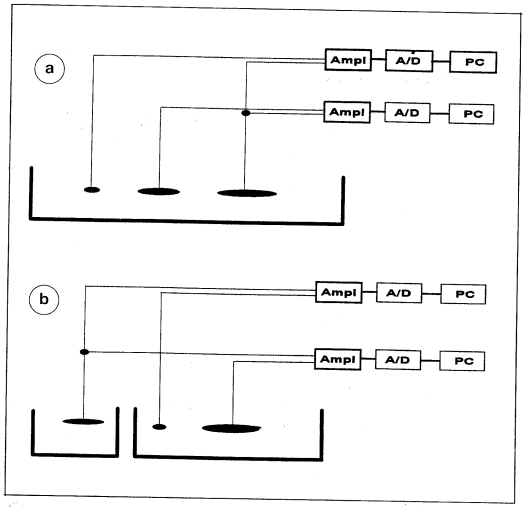

Fig. 2a,b. Electric line configurations with analog device, A/D converter and PC in Bar-Giora experiments.

2.2. *Experiments with different sized electrodes*

During 1994-1995 the above approach was tested at the Bar-Giora magnetic observatory where 30, 15 and 8 cm, disk-shaped, lead electrodes were installed at a depth of 25-30 cm. The reason for the shallow depth was to obtain the greatest effects associated with meteorological conditions. The configuration of the experimental system is shown in fig. 2a,b, where three electrodes are placed in one and two holes (first and second experiments respectively).

2.2.1. Electric potential – Radius dependency

Potential differences were compared using three electrodes of 30, 15 and 8 cm diameter placed in one and two holes about 1 m apart

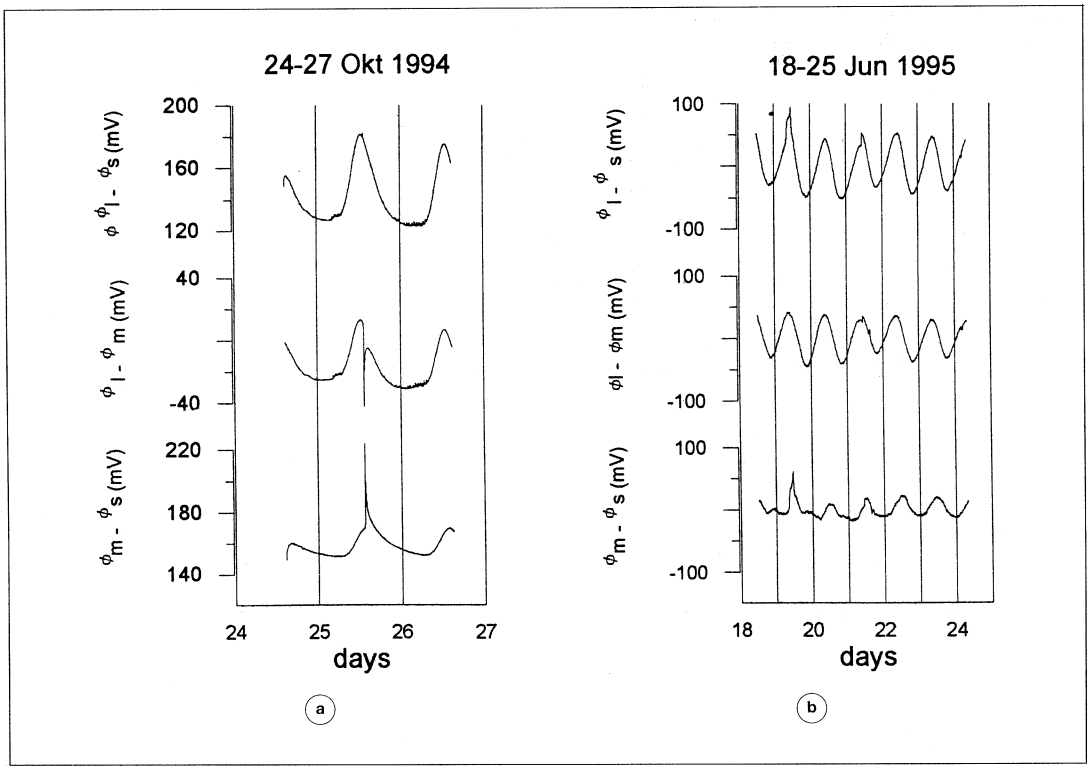

Fig. 3a,b. Electric potential variations between different size electrodes deployed in one hole.

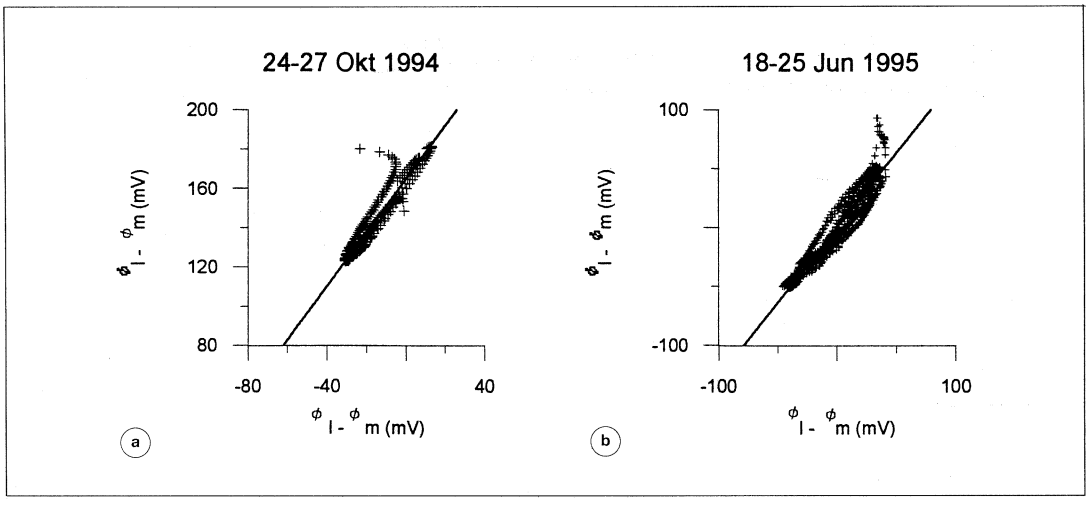

Fig. 4a,b. Potential difference interdependency of various sized electrodes and linear fit.

(Experiment I). Figure 3a,b shows records of the potential difference between large-small, large-medium and medium-small (top to bottom) electrodes over two periods. Strong daily periodic variations represent influences of meteorological changes on the ELV (variations in σ_0 in eq. (2.4)). All records are shown after trend removal. The spike changes on October 25, 1995 in the second channel were probably caused by noise in the electronic circuit. Suppose there is a proportional dependence between the electric potential and the radius of the electrodes, then the ratio is:

$$(\Phi_l - \Phi_s)/(\Phi_l - \Phi_m) = (r_l - r_s)/(r_l - r_m) = 1.47 \quad (2.5)$$

where the subscripts l, m and s denote large, medium and small electrodes, respectively.

The same ratio can be observed from measured potential differences. Figure 4a,b shows the relationship between $\Phi_l - \Phi_s$ and $\Phi_l - \Phi_m$ which are close to linear for October 1994 and June 1995. The relationships are not strong linear owing to the time delay between charge density changes of the different electrodes. The ratio given by eq. (2.5) was obtained using regression analysis and is similar to the theoretical estimations, *i.e.* about 1.4 and 1.3 for the periods October 24-26, 1994 and June 18-25, 1995, respectively. The empirical results are in agreement with the theory; eq. (2.4) is adequate for filtering the ELV.

2.2.2. Dependence on meteorological conditions

Two records of electric potential differences (Experiment II) are shown in fig. 5a,b where

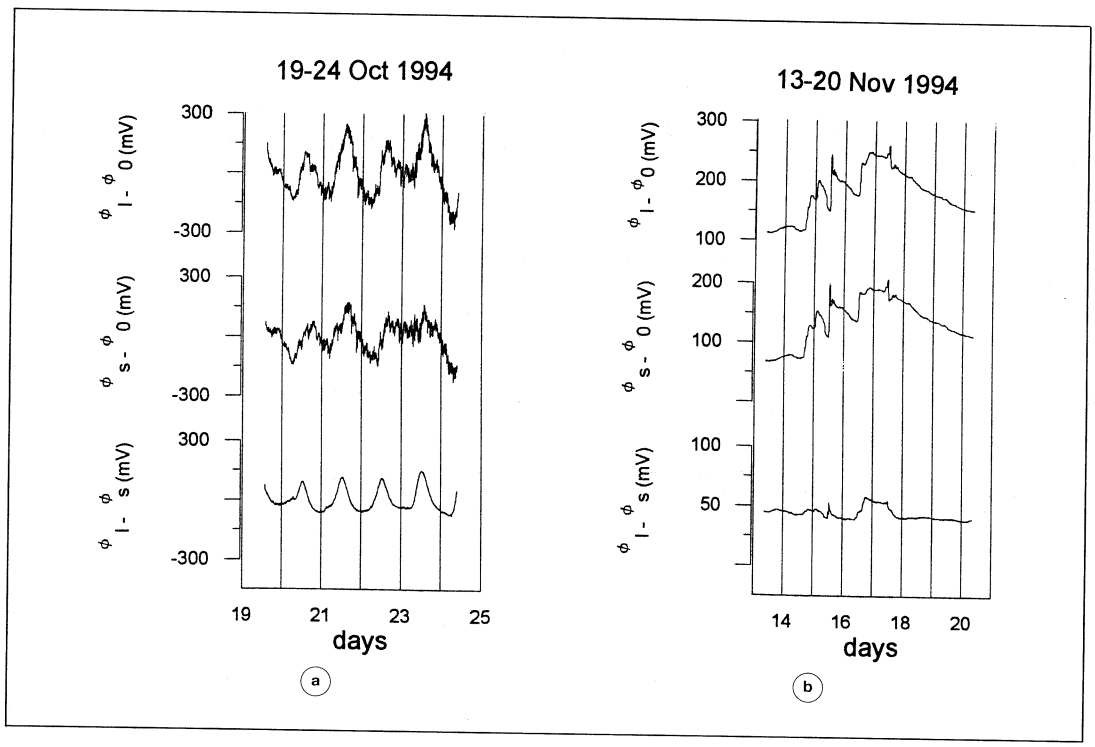

Fig. 5a,b. Potential differences between various sized electrodes on (a) sunny and (b) rainy days.

the two top graphs represent the potential difference between large (30 cm) and small (8 cm) electrodes installed in the same hole and a third electrode in another hole 10 m away. Signals of different sources are seen on the two top graphs; the bottom graphs are the computed residual of the two top graphs. These records were made under different meteorological conditions: sunny (fig. 5a) and rainy (fig. 5b) weather. The residual functions which represent the ELV show strong daily changes on sunny days and changes associated with rainfall. ELV are obviously strongly influenced by temperature and humidity.

3. Anthropogenic noise filtration (time-domain analysis)

3.1. *Quantity value determination of the noise indicator*

Analysis of anthropogenic noise shows the difference between specific industrial and natural noise signals and this distinctive feature formed the basis for an automated noise filtration process. Two intervals were selected in order to demonstrate our approach to anthropogenic noise filtration. The noise filtration process involves the following steps:

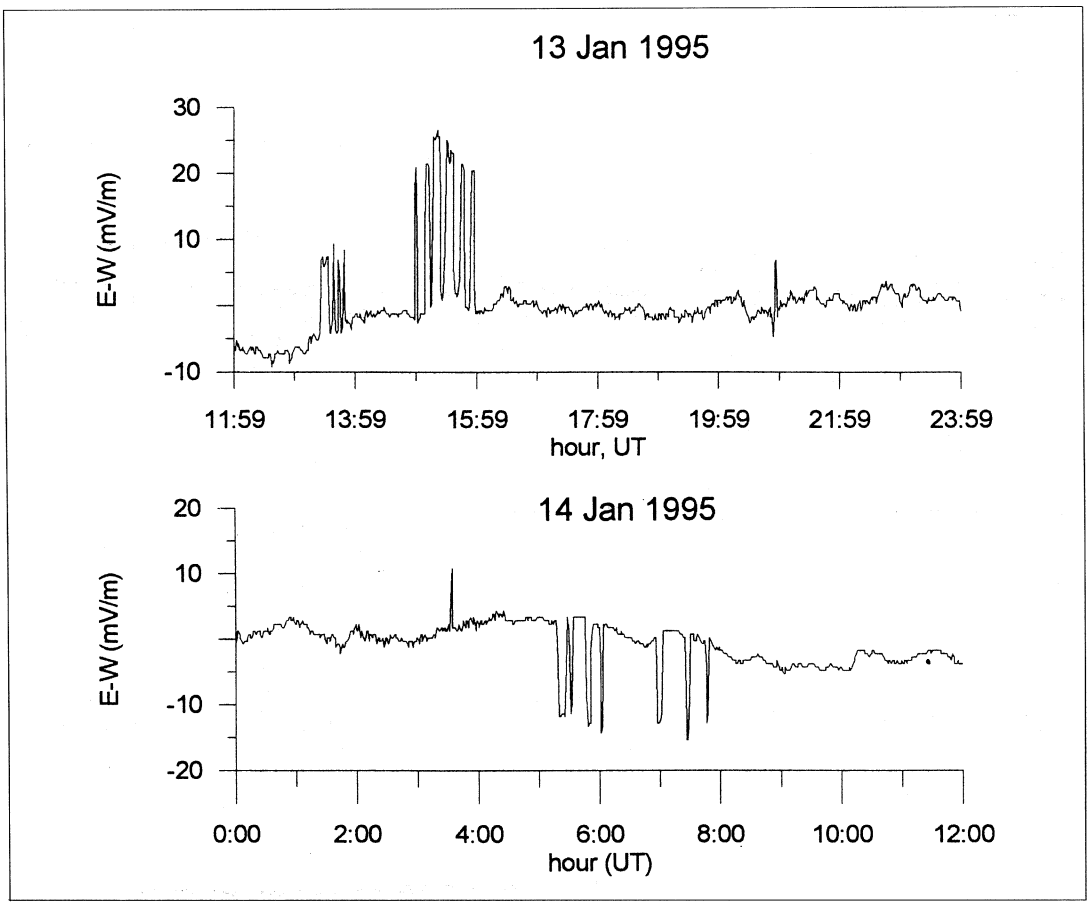

Fig. 6. Examples of anthropogenic noise recorded at the Bar-Giora observatory (east-west component).

a) *Quantity value determination of the noise indicator* – The anomalous changes in the electric field appeared at the Bar-Giora observatory at the beginning of 1994 and were caused by artificial sources. The changes start and finish quite abruptly and are of no more than two minutes duration (fig. 6). We used the first derivative as an indicator of this specific type of noise. Quiet signals, *i.e.* those uncontaminated by artificial noise, and their derivatives should fluctuate around zero. The density distribution of the derivative (or, precisely, the average value of the derivative of all two minute intervals) follows the normal distribution (see fig. 7). Based on this observation we defined the rate of change of the electric field of $\pm$ 7 μV/(m $\cdot$ min) as the threshold above which the signal should be considered noisy.

b) *Determination of noise intervals* – The distribution of anthropogenic noise does not follow normal distribution; hence all intervals which exceeded the limit of $\pm$ 7 μV/(m $\cdot$ min) were marked and eliminated from the records.

c) *Linear interpolation under noise intervals* – Eliminated noise signals were substituted by data obtained using linear interpolation. The results of anthropogenic noise filtration are shown in fig. 8a,b.

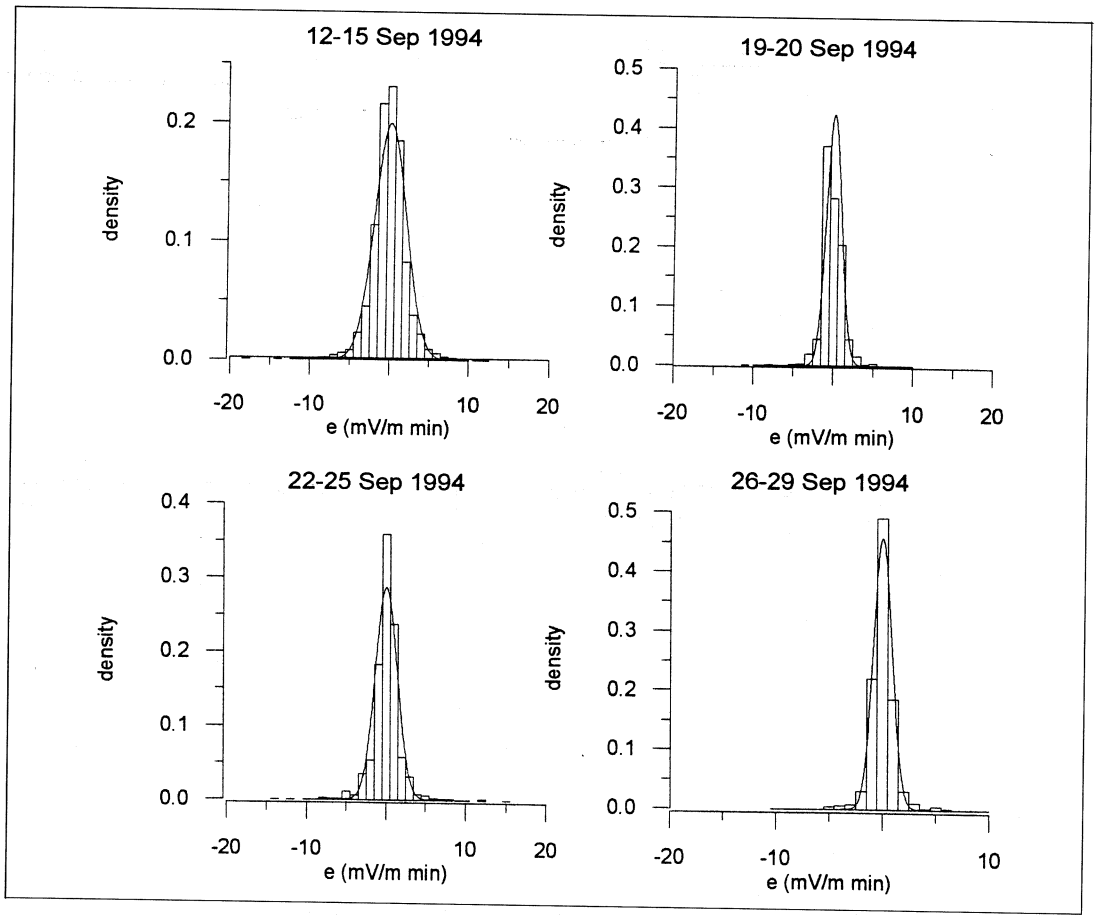

Fig. 7. Density distribution of the electric field derivative.

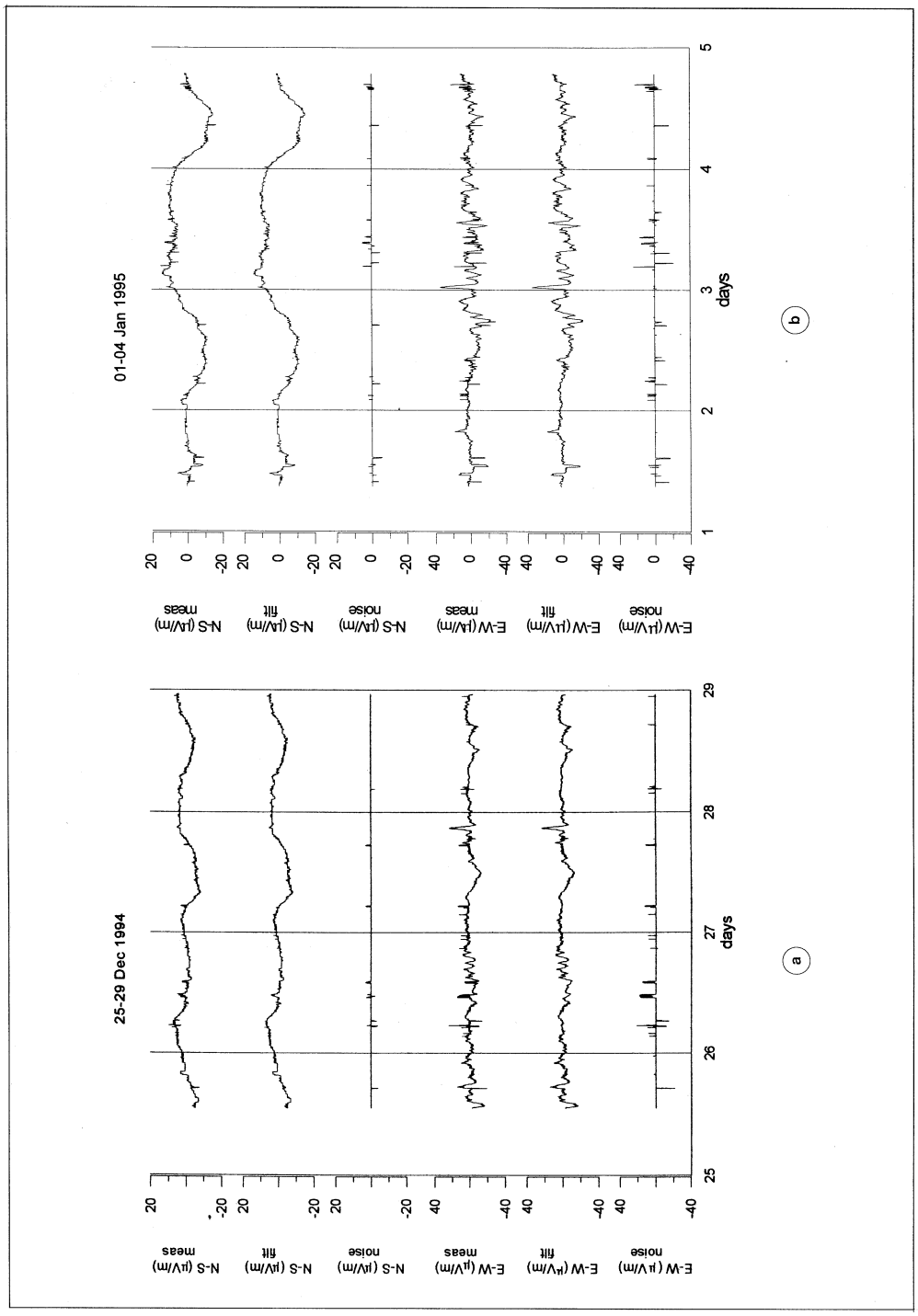

Fig. 8a,b. N-S and E-W electric field components recorded at the Bar-Giora observatory, filtered records and anthropogenic noise.

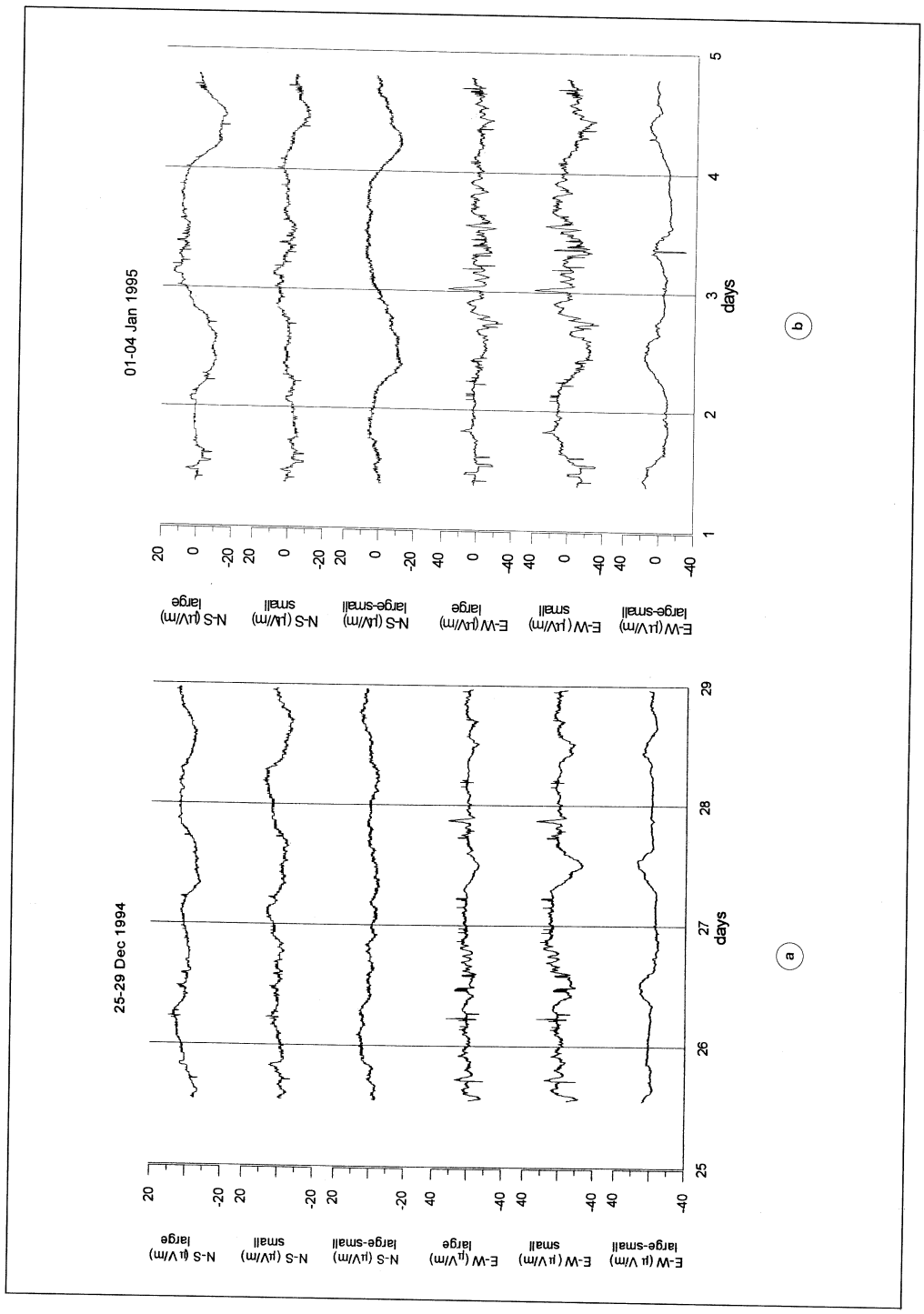

Fig. 9a,b. Electrotelluric field records obtained using two different sized electrodes and their residuals.

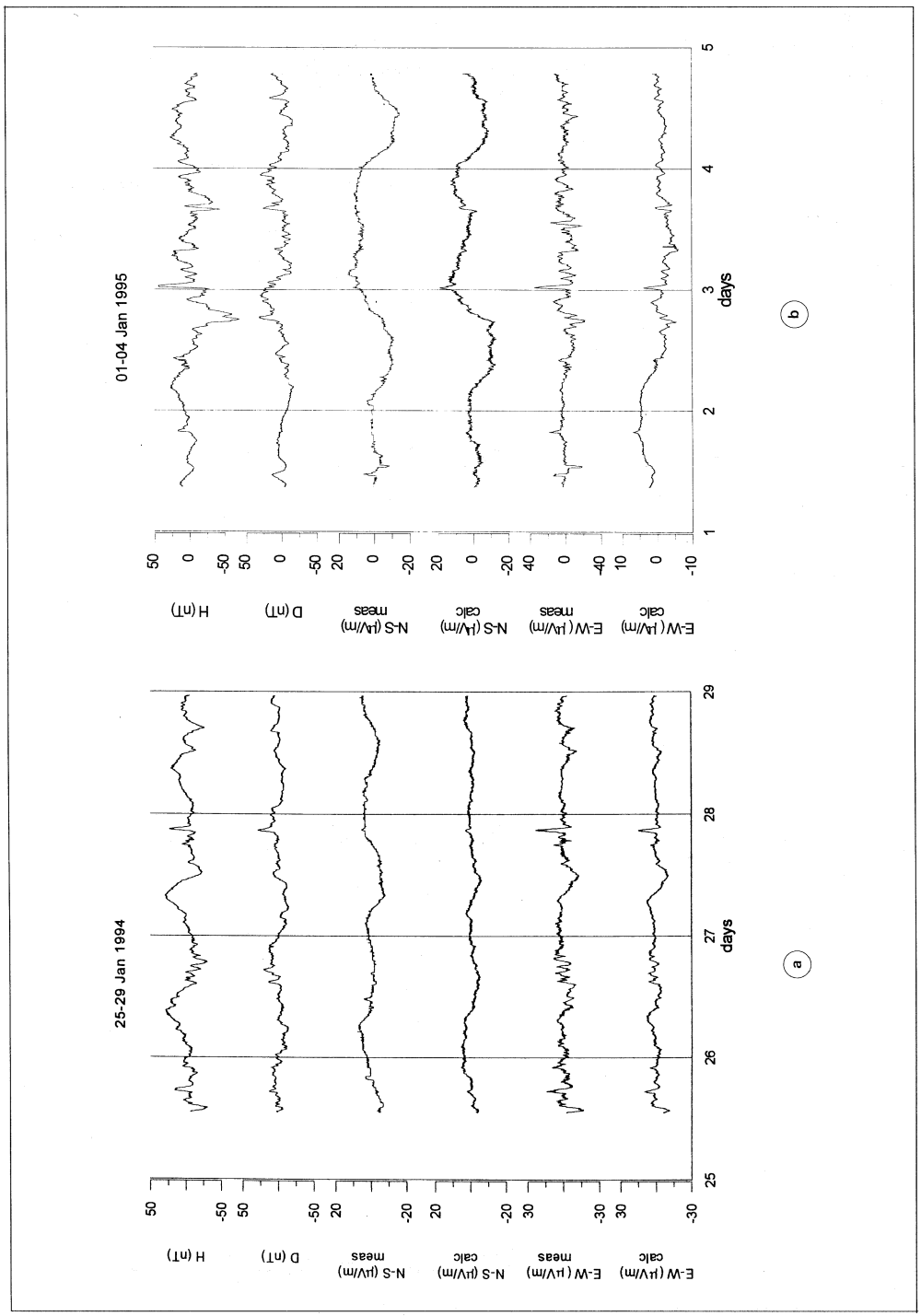

Fig. 10a,b. Horizontal components of the recorded magnetic field, measured and calculated electric field.

4. Filtration of external and local electrochemical sources

Suppose that the observed electric field consists of magnetotelluric and electrochemical sources. We based our calculations on electrotelluric field observations using two disk-shaped electrodes of different sizes. It was observed that records of the potential difference between two adjacent electrodes represent the electrochemical electric field changes. Assuming that the change density σ_0 in eq. (2.4) is identical for two adjacent electrodes, the electrochemical potential of the large electrode could be expressed by the potential difference between the large and small electrodes:

$$\Phi_l = r_l(\Phi_l - \Phi_s)/(r_l - r_s) \qquad (4.1)$$

With this result we can obtain the potential difference (for example) between E-W electrodes:

$$\Phi_l^{\mathrm{E}} - \Phi_l^{\mathrm{W}} = \frac{r_l}{r_l - r_s}\left((\Phi_l^{\mathrm{E}} - \Phi_l^{\mathrm{W}}) - (\Phi_s^{\mathrm{E}} - \Phi_s^{\mathrm{W}})\right) \qquad (4.2)$$

Two examples in fig. 9a,b represent electrochemical changes between large and small electrodes. The coefficient on the right hand side of eq. (4.2) can differ in theoretical value. In order to estimate this, substitute an electric field describing electrochemical changes in the magnetotelluric equation:

$$\begin{aligned} E_{x,i} &= Z_{xx} H_{x,i} + Z_{xy} H_{y,i} + C_x \varepsilon_{x,i} \\ E_{y,i} &= Z_{yx} H_{x,i} + Z_{yy} H_{y,i} + C_y \varepsilon_{y,i} \end{aligned} \qquad (4.3)$$

where $H_{x,i}$, $H_{y,i}$, $E_{x,i}$, $E_{y,i}$, $\varepsilon_{x,i}$, $\varepsilon_{y,i}$ are spectral components of magnetic, total electric and electrochemical parts of electric fields for the i-th measurement, respectively, and Z_{xx}, Z_{xy}, Z_{yx}, Z_{yy} and C_x, C_y are spectral components of impedance tensor and electrochemical coefficients.

The most commonly used approach to impedance tensor calculations is the least squares method (Sims *et al.*, 1971). The conditions for minimum error (differences between the left and right parts of eq. (4.3)) are realized when the derivative of errors with respect to the real and imaginary parts of the impedance elements and the electrochemical coefficients are equal to zero. This yields a system of ten linear equations from which we obtain, using the Gauss-Jordan method, ten unknowns (the real and imaginary parts of the four impedance elements and two electrochemical coefficients). These coefficients were used to calculate the electric field from the known magnetic and electrochemical part of the electric field.

Measured and calculated electric fields were compared in order to identify disturbances related to seismotectonic processes. Figure 10a,b show the same examples of calculated and observed electric fields (after industrial noise filtration) at the Bar-Giora observatory together with the magnetic field. The comparison also shows the correlation between measured and calculated variations.

5. Conclusions

1) Electrotelluric field variations obtained using two disk-shaped electrodes of differing size facilitate the identification of local electrochemical noise which, in turn, can be used as an empirical filter to clean the signals.

2) Time domain analysis is effective in reducing the effect of artificial noise.

Acknowledgements

The authors would like to thank the staff of the IPRG Seismology Division and the Research Department of the Survey of Israel for providing the electrotelluric and geomagnetic monitoring.

This work was sponsored by the Ministry of Science and Technology.

REFERENCES

DI BELLO, G., V. LAPENNA, C. SATRIANO and V. TRAMUTOLI (1994): Self-potential time series analysis in a seismic area of the Southern Apennines: preliminary results, *Annali di Geofisica*, **37**, 1137-1148.

JACKSON, J.D. (1962): *Classical Electrodynamics*, New York, London.

KINOSHITA, M., M. UYESHIMA and S. UYEDA (1989): Earthquake prediction by means of telluric potential monitoring. Progress Report 1: Installation of monitoring network, *Bull. Earthquake Res. Inst.* (University of Tokyo), **64**, 255-311.

MARON, C., G. BAUBRON, L. HEBRETEAU and B. MASSINON (1993): Experimental study of a VAN network in the French Alps, *Tectonophysics*, **224**, 51-81.

SHIRMAN, B. and A. SHAPIRA (1994): Feasibility of geomagnetic earthquake prediction in Israel, Annual Report, Results of Investigations (August 1993 to July 1994), *IPRG Report* 328/507/93(2).

SIMS, W.E., F.X. BOSTICK and H.W. SMITH (1971): The estimation of magnetotelluric impedance tensor elements from measured data, *Geophysics*, **36**, 938-942.

VAROTSOS, P. and K. ALEXOPOULOS (1984a): Physical properties of the variations of the electric field of the Earth preceding earthquakes I, *Tectonophysics*, **110**, 73-98.

VAROTSOS, P. and K. ALEXOPOULOS (1984b): Physical properties of the electric field of the Earth preceding earthquakes II, Determination of epicenter and magnitude, *Tectonophysics*, **110**, 99-125.